Environmental Science & Technology

pubs.acs.org/est

Article

Electron Hopping Enables Rapid Electron Transfer between Quinone-/Hydroquinone-Containing Organic Molecules in Microbial Iron(III) Mineral Reduction

Yuge Bai,[‖] Tianran Sun,[‖] Largus T. Angenent, Stefan B. Haderlein, and Andreas Kappler*

Cite This: *Environ. Sci. Technol.* 2020, 54, 10646−10653

Read Online

ACCESS | Metrics & More | Article Recommendations | Supporting Information

ABSTRACT: The mechanism of long-distance electron transfer via redox-active particulate natural organic matter (NOM) is still unclear, especially considering its aggregated nature and the resulting low diffusivity of its quinone- and hydroquinone-containing molecules. Here we conducted microbial iron(III) mineral reduction experiments in which anthraquinone-2,6-disulfonate (AQDS, a widely used analogue for quinone- and hydroquinone-containing molecules in NOM) was immobilized in agar to achieve a spatial separation between the iron-reducing bacteria and ferrihydrite mineral. Immobilizing AQDS in agar also limited its diffusion, which resembled electron-transfer behavior of quinone- and hydroquinone-containing molecules in particulate NOM. We found that, although the diffusion coefficient of the immobilized AQDS/AH_2QDS was 10 times lower in agar than in water, the iron(III) mineral reduction rate (1.60 ± 0.28 mmol $L^{-}1$ Fe(II) d^{-1}) was still comparable in both media, indicating the existence of another mechanism that accelerated the electron transfer under low diffusive conditions. We found the correlation between the heterogeneous electron-transfer rate constant (10^{-3} cm s^{-1}) and the diffusion coefficient (10^{-7} cm^2 s^{-1}) fitting well with the "diffusion-electron hopping" model, suggesting that electron transfer via the immobilized AQDS/AH_2QDS couple was accomplished through a combination of diffusion and electron hopping. Electron hopping increased the diffusion concentration gradient up to 10^6-fold, which largely promoted the overall electron-transfer rate during microbial iron(III) mineral reduction. Our results are helpful to explain the electron-transfer mechanisms in particulate NOM.

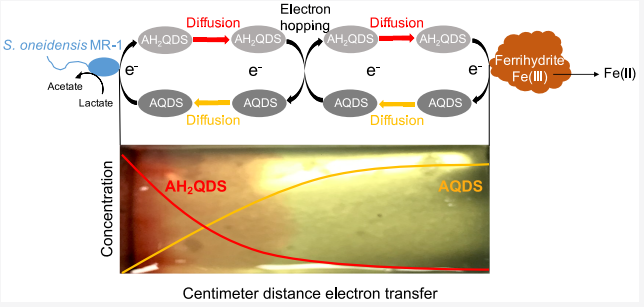

INTRODUCTION

Natural organic matter (NOM) is a complex mixture of organic molecules that are primarily derived from the decay of plant and microbial residues, and it makes up a major fraction of organic matter in soils and sediments.[1] Based on the particle size that is operationally defined by filtering through 0.45 μm cutoff filters, NOM is categorized into dissolved NOM and particulate NOM.[2] Due to the presence of redox-active moieties such as quinone and hydroquinone, NOM is known to undergo redox cycles thus acting as an electron shuttle and transferring electrons between spatially separated Fe(III) minerals and Fe(III)-reducing bacteria.[3−5] Such an electron shuttling process by NOM has been shown to help Fe(III)-reducing bacteria to overcome the respiratory challenge and perform extracellular electron transfer in anoxic soils and sediments.[6]

Dissolved NOM is usually homogeneously distributed in pore waters and possesses a high diffusivity[7] with a measured diffusion coefficient (D_0) of 10^{-6} cm^2 s^{-1}. This diffusion coefficient is in the same order of magnitude as the D_0 of a variety of biological electron shuttle molecules (i.e., flavin mononucleotide[8] and pyocyanin[9]) that are known to diffusively transfer electrons up to a 100 micrometer (μm) distance.[10] In contrast to dissolved NOM, particulate NOM has a much lower physical mobility and commonly accumulates in the solid phase of soils and sediments due to aggregation and coprecipitation.[11] Similar as for dissolved NOM, a stimulation of microbial Fe(III) reduction through electron transfer facilitated by NOM redox cycling has also been observed for particulate NOM.[5,12,13] Given the environmental abundance, particulate NOM was proposed to be able to transfer electrons across centimeter (cm) distances.[5,13] Such long-distance electron transfer can bridge energy and matter exchange across liquid and solid interphases in anoxic soils and sediments. However, the underlying mechanisms that enable the occurrence of long-distance electron transfer of particulate NOM remain unclear. Whereas some studies emphasized the

Received: April 21, 2020
Revised: July 15, 2020
Accepted: July 27, 2020
Published: July 27, 2020

https://dx.doi.org/10.1021/acs.est.0c02521
Environ. Sci. Technol. 2020, 54, 10646−10653

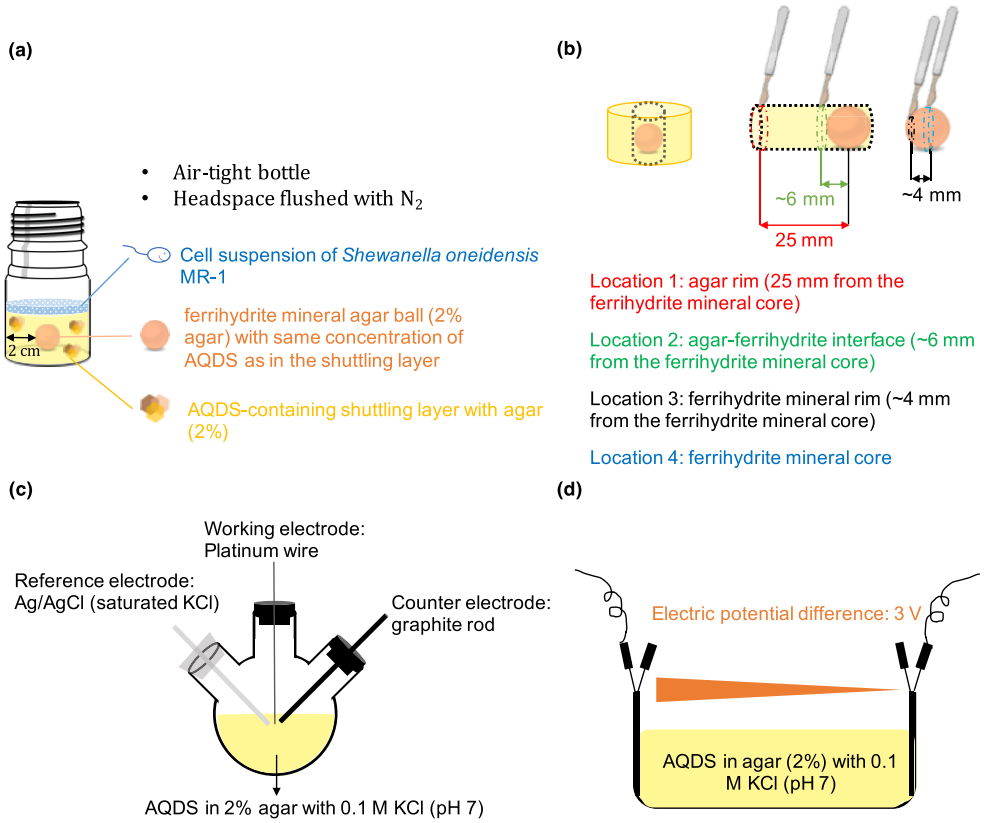

Figure 1. Cell suspension incubation system that separates *S. oneidensis* MR-1 and ferrihydrite by a 2 cm distance with AQDS as an electron shuttle (a). At each sampling point, an agar slice with 1 mm thickness was taken at four locations in an anoxic glovebox (100% N_2) (b). The cyclic voltammetry of AQDS was measured in a Biologic model VSP potentiostat controlled by the EC-lab platform at room temperature in a three-electrode-configured cell at pH 7 (c). The two-electrode-configured electrochemical cell ($L \times W \times H = 5 \times 3 \times 2$ cm) used to investigate the maximum electron-transfer distance of AH_2QDS after electrochemical reduction of AQDS (d).

importance of dissolved NOM serving as a mediator that diffusively transfers electrons between particulate NOM molecules,[14] others proposed the formation of an electron-transfer network by particulate NOM, as it could also be formed by bacterial nanowires,[15] to transfer electrons over cm distances.[16]

It has been proven that quinone- and hydroquinone-containing molecules dominated the electron-transfer properties of particulate NOM. However, their diffusivity is much lower than that of dissolved NOM, due to the precipitating nature of particulate NOM. To advance our understanding of the electron-transfer mechanism of particulate (solid-phase) NOM, we used anthraquinone-2,6-disulfonate (AQDS), as an analogue for quinone-containing particulate NOM molecules, and AH_2QDS that was generated from the microbial reduction of AQDS, as an analogue for the hydroquinone-containing molecules in particulate NOM. By immobilizing AQDS in agar (2%), we mimicked the diffusion limitation of quinone-/hydroquinone-containing molecules in particulate NOM. We would like to note that we are aware of the fact that the AQDS/AH_2QDS couple was not fully immobilized, but instead, its diffusivity was reduced to simulate the electron-transfer conditions relevant for particulate NOM. However, for simplicity we termed this reduced diffusion condition as "immobilized" throughout the manuscript. This AQDS−agar mixture was placed in an incubation system that physically separated the Fe(III)-reducing bacteria (*Shewanella oneidensis* MR-1) and ferrihydrite by 2 cm to inhibit direct microbial ferrihydrite reduction. We hypothesized that electron hopping (i.e., the electron self-exchange reaction occurring between closely compacted redox centers[17]) plays a critical role in the electron transfer between immobilized AQDS and AH_2QDS molecules and accelerates microbial Fe(III) mineral reduction.

MATERIALS AND METHODS

Cell Suspension Experiment. Microbial ferrihydrite reduction was carried out in a cell suspension incubation system for which AQDS was immobilized in agar, and *S. oneidensis* MR-1 (10^8 cells mL^{-1}) and ferrihydrite (15 mmol L^{-1}) were separated by a distance of 2 cm (Figure 1a). The concentrations of AQDS in agar were 5 mmol L^{-1}, 10 mmol L^{-1}, 25 mmol L^{-1}, or 50 mmol L^{-1}. The pore size of the agar (2%) was 100−200 nm,[18] which is small enough to prevent microbes from penetration and therefore from direct contact to ferrihydrite.[19] Phosphate buffer (5 mmol L^{-1}, pH 7.0−7.2) was used in the incubation. Although phosphate can lead to the formation of Fe(II)-phosphate minerals such as vivianite, this buffer was chosen to allow comparison of our study to previous studies.[20−22] More detailed information about the setup of the cell suspension incubation can be found in our previous study.[19] For analysis, agar samples from each treatment were taken in triplicates in an anoxic glovebox (100% N_2). A 10 mL syringe, cut at the top, was used to take a core from the agar for quantifying the Fe concentration. Agar slices (1 mm thickness for each slice) were taken from locations 1, 2, 3, and 4 of the core as designed in Figure 1b. After dissolving in 1 M HCl for

https://dx.doi.org/10.1021/acs.est.0c02521
Environ. Sci. Technol. 2020, 54, 10646−10653

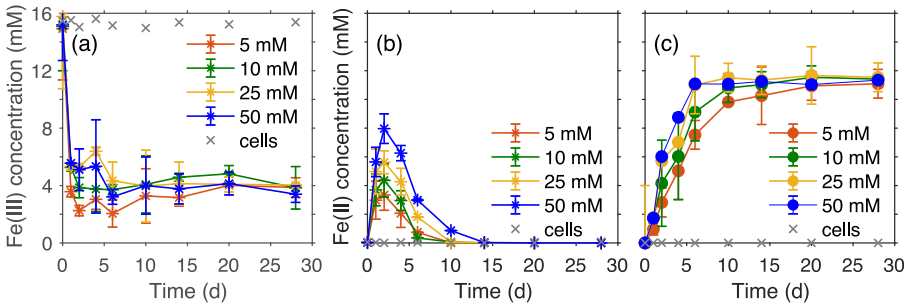

Figure 2. Fe(III) (a) and Fe(II) (b) concentrations measured at the ferrihydrite-mineral rim (location 3) and (c) Fe(II) concentration over time at the agar-ferrihydrite interface (location 2) of the 15 mM ferrihydrite reduction by 10^8 mL^{-1} *S. oneidensis* MR-1 in the presence of 15 mM lactate as the electron donor amended with either 5 mmol L^{-1} (red), 10 mmol L^{-1} (green), 25 mmol L^{-1} (yellow), or 50 mmol L^{-1} (blue) anthraquinone-2,6-disulfonate (AQDS) as the electron shuttle. All experiments were conducted in the cell suspension incubation system at 30 °C in the dark. Data points shown are mean values from triplicate bottles ±SD.

1 h, the Fe(II) and Fe(III) concentrations in each slice were quantified using the spectrophotometric ferrozine assay.[23,24]

Electrochemical Analysis. Cyclic voltammetry was performed to investigate the redox cycling of the AQDS/AH_2QDS couple that was immobilized in agar. Potassium chloride (KCl, 0.1 mol L^{-1}) was added as a supporting electrolyte, and potassium phosphate (5 mmol L^{-1}) was used to buffer the pH at 7.0−7.2. Cyclic voltammetry was carried out in a three-electrode-configured electrochemical cell for which platinum wire, a graphite rod, and Ag/AgCl (sat. KCl) were used as a working, counter, and reference electrode, respectively (Figure 1c). The AQDS concentration was 5 mmol L^{-1}, 10 mmol L^{-1}, 15 mmol L^{-1}, 25 mmol L^{-1}, or 50 mmol L^{-1} to have the same conditions as in the microbial Fe(III) mineral reduction incubations. Potential scan rates ranged from 50 mV s^{-1} to 300 mV s^{-1}.

A two-electrode-configured electrochemical cell ($L \times W \times H$ = 5 × 3 × 2 cm, Figure 1d) was used to investigate the maximum transfer distance of AH_2QDS after electrode reduction of AQDS. The initial AQDS concentration was 25 mmol L^{-1} or 50 mmol L^{-1}. KCl (0.1 mol L^{-1}) and phosphate (5 mmol L^{-1}) were added as a supporting electrolyte and pH buffer (7.0−7.2), respectively. Carbon paper was used as both a working and counter electrode. A constant voltage (i.e., the potential difference between working and counter electrodes) of 3 V was applied to the electrochemical cell, which was also the tested lowest voltage that was able to initiate the reduction of AQDS in this particular cell configuration. During the experiment, we did not observe any gas bubbles evolving from the electrodes, suggesting that the applied voltage was high enough to drive AQDS reduction but still below the voltage threshold for water splitting.

At the end of the experiment, we quantified AQDS and AH_2QDS concentrations using a spectrophotometric method. The agar slices (thickness 1 mm) were put into an electroporation cuvette (BTX, 45-0134), and the absorbance of the agar slices at the wavelength from 200 to 550 nm was measured with a fluorescence spectrophotometer (FluoroMax-4, Jobin Yvon-SPEX instruments, New Jersey, USA). Pure agar (2%) with 5 mmol L^{-1} phosphate buffer and 0.1 mol L^{-1} KCl was used as a blank. The peak positions of AQDS (320 nm) and AH_2QDS (400 nm) are in accordance with previously reported values.[25] We quantified AQDS concentrations based on the concentration-peak height curve of standard samples and estimated the concentrations of AH_2QDS through the decrease of AQDS by assuming all decreased AQDS was converted to AH_2QDS. For example, in the experiment with an initial AQDS concentration of 25 mmol L^{-1}, we found a 7.2 mmol L^{-1} loss of AQDS, which suggests the formation of 7.2 mmol L^{-1} AH_2QDS. The same approach was applied to the experiment with initial AQDS concentrations of 50 mmol L^{-1}, in which a 33.7 mmol L^{-1} AQDS loss, thus, 33.7 mmol L^{-1} AH_2QDS formation, was detected.

RESULTS AND DISCUSSION

Immobilized AQDS Enables Microbial Ferrihydrite Reduction Across a 2 cm Distance. Our incubations showed that after accepting electrons from microbial metabolism, AQDS was reduced to AH_2QDS, which subsequently transferred electrons to ferrihydrite. In the incubation with 5 mmol L^{-1} immobilized AQDS in agar, the Fe(III) concentration at the ferrihydrite-mineral rim (i.e., location 3 in Figure 1b) decreased from 14.92 mmol L^{-1} to 3.04 mmol L^{-1} within the first 2 days of incubation (Figure 2a). Inversely, the Fe(II) concentration at the same location increased from 0 mmol L^{-1} to 3.34 mmol L^{-1} (Figure 2b). However, after 2 days, the Fe(II) concentration at the ferrihydrite-mineral rim started to decrease, and its final concentration was stabilized at 0.74 mmol L^{-1} after 10 days of incubation. This Fe(II) concentration decrease at the ferrihydrite-mineral rim (location 3) was likely caused by sorption of Fe(II) onto the ferrihydrite, which dissolved over time and diffused across the agar-ferrihydrite interface (i.e., location 2) into the bulk of agar. As a result, the Fe(II) concentration at the agar-ferrihydrite interface increased from 0.96 mmol L^{-1} to 10.02 mmol L^{-1} within 10 days of incubation (Figure 2c). No Fe(II) was detected at the agar rim (i.e., location 1, Figure 1b) during the entire incubation period (SI Figure S1a). This was probably due to the interaction of Fe(II) and phosphate by the formation of Fe(II)-phosphate minerals, such as vivianite,[19,26−28] that impeded further diffusion of Fe(II) in the agar.

Consistent with the 5 mmol L^{-1} AQDS experiment, also 10 mmol L^{-1}, 25 mmol L^{-1}, and 50 mmol L^{-1} of immobilized AQDS initiated ferrihydrite reduction from the ferrihydrite-mineral rim (location 3) and accumulated Fe(II) in the form of Fe(II)-phosphate minerals (i.e., vivianite) at the agar-ferrihydrite interface (location 2) (Figure 2c). However, it should be noticed that a diffusion-reaction model developed in our previous study[19] showed that the formation of Fe(II)-phosphate minerals should co-occur at the agar-ferrihydrite interface (location 2) and ferrihydrite-mineral rim (location 3).

https://dx.doi.org/10.1021/acs.est.0c02521
Environ. Sci. Technol. 2020, 54, 10646−10653

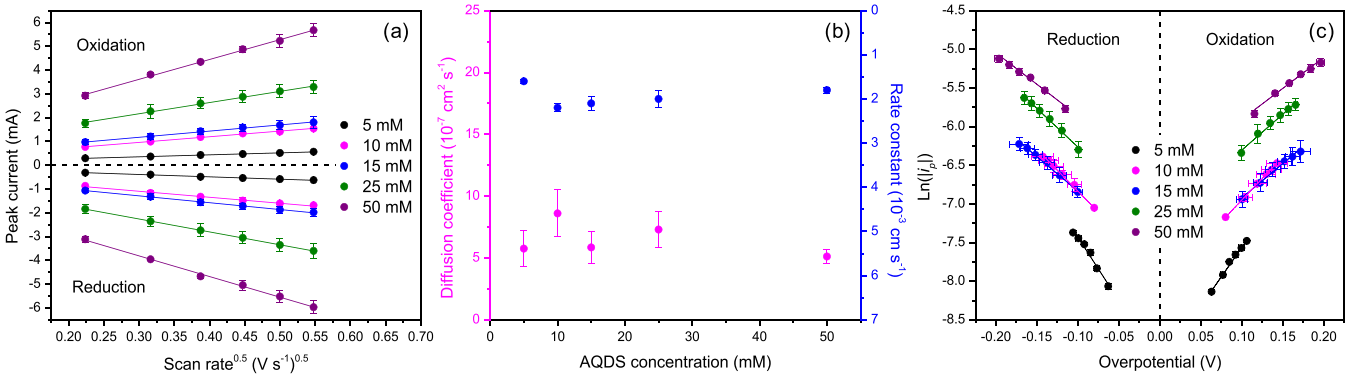

Figure 3. Linear dependency of peak current on square root of potential scan rate for different AQDS concentrations in agar (a). The calculated diffusion coefficient D_0 (pink) and heterogeneous electron-transfer rate constant k_0 (blue) of AQDS in agar (b). The Tefal plot showing the linear relationship between the natural logarithm of the absolute value of the peak current (ln|i_p|) and overpotential (i.e., difference between peak potential and formal potential) at different potential scan rates (c). Original cyclic voltammograms from which Figure 3 was derived can be found in Figure S4.

The observation of the accumulation of Fe(II)-phosphate minerals only at the agar-ferrihydrite interface might be caused by the difficulties visually observing the boundary of the ferrihydrite-mineral core to the clean agar during the sampling procedure.

Although higher concentrations of AQDS lead to higher extents of ferrihydrite reduction, and therefore more Fe(II) formation at the ferrihydrite-mineral rim, the ferrihydrite reduction never reached the ferrihydrite-mineral core (i.e., location 4 in Figure 1b), which was shown by the stable Fe(III) concentration between 14 mmol L^{-1} to 16 mmol L^{-1} at this location (SI Figure S2c). Similar phenomena of incomplete ferrihydrite reduction were also reported in previous studies.[29,30] We attribute the incomplete reduction in our system to the accumulation of Fe(II)-phosphate minerals at the agar-ferrihydrite interface and ferrihydrite-mineral rim, thus reducing the thermodynamic driving force of ferrihydrite reduction[31] and limiting the acceptance of electrons.[27]

With 5 mmol L^{-1}, 10 mmol L^{-1}, 25 mmol L^{-1}, and 50 mmol L^{-1} AQDS immobilized in agar, the average ferrihydrite reduction rates were 1.25 ± 0.05 mmol L^{-1} Fe(II) d^{-1}, 1.52 ± 0.16 mmol L^{-1} Fe(II) d^{-1}, 1.76 ± 0.07 mmol L^{-1} Fe(II) d^{-1}, and 1.88 ± 0.11 mmol L^{-1} Fe(II) d^{-1}, respectively (SI Figure S3). During our previous study, we showed that the diffusion coefficient of AQDS was 10^{-7} cm^2 s^{-1} in agar,[19] which is about ten times lower than that in water (10^{-6} cm^{2}s^{-1}).[32,33] However, the ferrihydrite reduction rate of the incubations with AQDS immobilized in agar was comparable and in the same order of magnitude than in water (2.36 ± 1.07 mmol L^{-1} Fe(II) d^{-1}).[34] These results indicated that other electron-transfer mechanisms existed in addition to diffusion, which enhanced the overall AQDS electron-transfer rate in agar.

Electron Hopping Enhanced AQDS Diffusion. Electron hopping between adjacent redox centers has been reported in many materials and dominates the solid-phase electron transfer when molecular diffusivity is low or absent. Several theories and models, notably the Dahms-Ruff model,[35−37] the Blauch-Saveant model,[38] and the Marcus−Hush theory,[39,40] have been established and used to explain the electron hopping in redox-active polymers.[41] Electron hopping has been shown to be involved in the electron-transfer process in microbial nanowires[42] and between the redox-active proteins in the extended membranes of *Shewanella oneidensis* MR-1.[43] To demonstrate electron hopping in the agar-immobilized AQDS/AH_2QDS couple, we performed cyclic voltammetry and observed two distinct peaks during the reduction (i.e., AQDS + 2e$^-$+ 2H$^+$ → AH_2QDS) and oxidation (i.e., AH_2QDS − 2e$^-$ − 2H$^+$ → AQDS) scans (SI Figure S4). The fact that the peak current ratio of reduction and oxidation scans was equal to unity and independent of the scan rate (Figure 3a) indicated that there were no parallel chemical reactions that were coupled to the electron transfer of either AQDS or AH_2QDS. The formal potential (i.e., the average of peak potentials) was determined at −0.3 V (vs SHE, SI Figure S6) in agar, which is more negative to the previously reported standard reduction potential (−0.228 V)[25] and the formal potential (−0.185 V)[44] of AQDS in aqueous solution (at pH 7). The linear dependence of peak current on the square root of the applied potential scan rate (Figure 3a) complies with the Randles−Sevcik equation (eq 1)

$$i_p = 269000 \times n^{\frac{3}{2}} \times A \times D_0^{\frac{1}{2}} \times C \times \nu^{\frac{1}{2}} \quad (1)$$

$$D_0 = \left(\frac{Slope}{269000 \times n^{\frac{3}{2}} \times A \times C} \right)^2 \quad (2)$$

where i_p is the peak current, n (=2) is the number of transferred electrons by the AQDS/AH_2QDS couple, A (0.314 cm^2) is the electrode surface area, C is the initial AQDS concentration in bulk, ν indicates the potential scan rate, and D_0 is the diffusion coefficient. Our calculations use the same diffusion coefficient for AQDS and AH_2QDS due to their similar molecular structures and because of the symmetric peak current performance between the reduction scan of AQDS and the oxidation scan of AH_2QDS (SI Figure S4). A similar D_0 relationship was also observed between the 1,4-benzoquinone and 1,4-hydroquinone redox-couple.[45] From the slope of the linear plot of i_p as a function of $\nu^{0.5}$ (eq 2), we determined D_0 at 5.5 ± 3.2 × 10^{-7} cm^2 s^{-1} (average value of different AQDS concentrations, which is shown by the pink dots in Figure 3b). We further calculated the heterogeneous electron-transfer rate constant (k^0) of the AQDS/AH_2QDS couple, using eq 3 based on the observed wide separation of reduction and oxidation peak potentials shown in cyclic voltammograms[40]

https://dx.doi.org/10.1021/acs.est.0c02521
Environ. Sci. Technol. 2020, 54, 10646−10653

$$k^0 = \frac{e^{Intercept}}{0.227 \times n \times F \times A \times C} \quad (3)$$

in which the intercept was obtained from a linear fit of the natural logarithm of the absolute value of the peak current ($\ln|i_p|$) and overpotential (i.e., difference between peak potential and formal potential, SI Figure S7) at different potential scan rates (Figure 3c). F is the Faraday constant, and the rest of the terms have the same meaning as in eqs 1 and 2. k^0 was determined at $1.9 \pm 0.2 \times 10^{-3}$ cm s^{-1} (average value for different AQDS concentrations, as shown by blue dots in Figure 3b). Both k^0 and D_0 remained relatively constant from low to high AQDS concentrations.

The correlation between k^0 and D_0 well fitted with the diffusion-electron hopping model that was recently developed to explain the electron transfer in a nonconjugated polymer.[46] In the diffusion-electron hopping model, the overall electron transfer is controlled by diffusion (D_0), which determines the electron-transfer rate (k^0) through a function of $k^0 = \kappa_{el}\frac{3D_0}{2L}\exp\left(-\frac{\lambda}{4k_bT}\right)$ (κ_{el}, electron transmission coefficient; L, mean free distance; λ, reorganization energy; k_b, Boltzmann constant; T, temperature). This fitting suggests that the overall electron transfer through immobilized AQDS/AH_2QDS was accomplished by a series of diffusion and electron hopping steps, which is shown between interfaces 1 and 2 in eq 4.

$$\begin{array}{l} Microbe + AQDS \xrightarrow{\quad} \overset{1}{\vert} AH_2QDS \xrightarrow{k_{diff}} AH_2QDS + AQDS \xrightarrow{k_{hp}} \\ \qquad\qquad\qquad\qquad\qquad\qquad\qquad\qquad\qquad\qquad \overset{2}{\vert} \\ AQDS + AH_2QDS \cdots\cdots AH_2QDS + ferrihydrite \end{array} \quad (4)$$

Interfaces 1 and 2 represent microbe-AQDS and AH_2QDS-ferrihydrite interfaces, respectively. Therefore, the overall electron-transfer rate constant ($k_{overall}$) can be described by a serial reaction equation based on the classical Noyes expression (eq 5)

$$\frac{1}{k_{overall}} = \frac{1}{k_{hp}} + \frac{1}{k_{diff}} \quad (5)$$

where k_{hp} indicates the rate constant of electron hopping between AQDS and AH_2QDS redox centers, and k_{diff} is the diffusion constant. It ought to be noted that here we employed the Noyes expression only for the purpose of qualitative description of the serial reaction concept and not for quantitative data fitting. This is because the Noyes expression is a mean field approach that applies to the electron-transfer situation in which diffusion is faster than electron hopping. As we show below, the overall electron transfer of the immobilized AQDS/AH_2QDS couple was an opposite regime to the Noyes expression, which was controlled by diffusion instead of electron hopping.

It is well-known that the reduction of AQDS to AH_2QDS is a two-electron-transfer step process, including the formation of a semiquinone radical (i.e., AQDS + e^- → AHQDS* + e^- → AH_2QDS). However, in our system, these two steps could not be distinguished as only one current peak appeared in either the oxidation or reduction cycle in the cyclic voltammograms (SI Figure S4). Therefore, the electron hopping rate constants, k_{hp}, reflected the overall kinetics of the two steps. We estimated k_{diff} (~10^6 L mol^{-1} s^{-1}) by using the Smoluchowski model: $k_{diff} = 16\pi D_0 \alpha N_A$ (α, radius of the redox centers (in the magnitude of nm, SI Figure S8); N_A, Avogadro constant). k_{hp} (~10^8 L mol^{-1} s^{-1}) was approximated by the linear fitting of k^0 and D_0

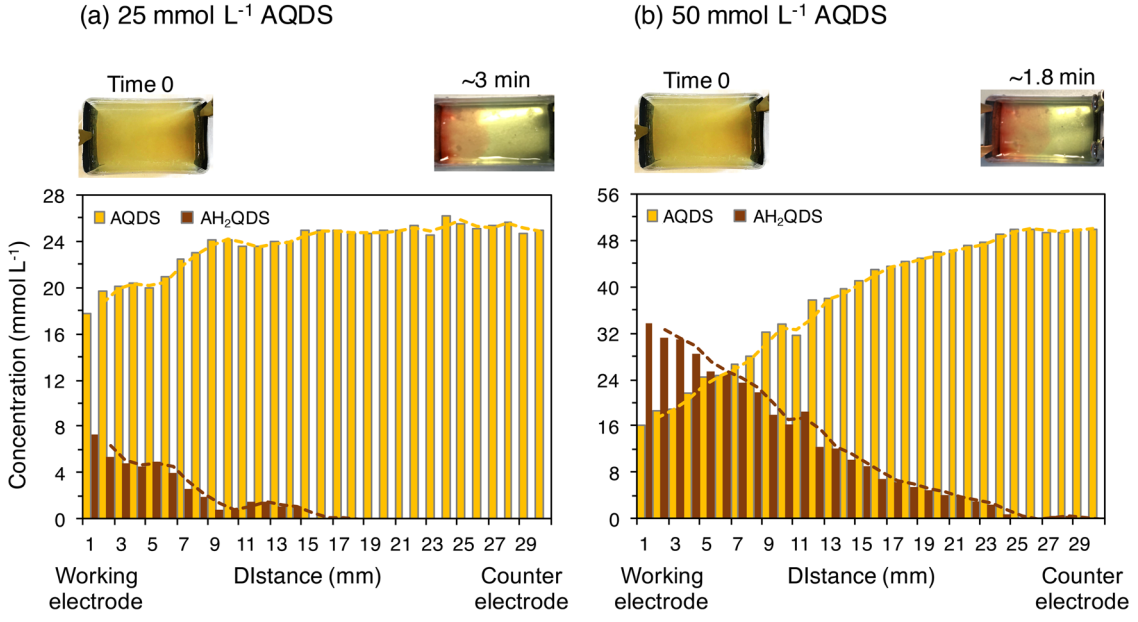

Figure 4. AQDS and AH_2QDS concentrations measured spectrophotometrically at each 1 mm in agar (2%) in the experiment with a two-electrode-configured electrochemical cell ($L \times W \times H = 5 \times 3 \times 2$ cm, Figure 1d). The initial AQDS concentration was 25 mmol L^{-1} (a) and 50 mmol L^{-1} (b). A voltage (i.e., the potential difference between working and counter electrodes) of 3 V was applied to initiate the reduction of AQDS. The produced AH_2QDS showed a bright orange color, and it expanded from the working electrode toward the counter electrode over time (as shown in the pictures above the bar plots). Once the expansion of AH_2QDS stopped, we recorded the time (3 and 1.8 min for the experiment with the initial AQDS concentration of 25 mmol L^{-1} and 50 mmol L^{-1}, respectively) and measured the AQDS and AH_2QDS concentrations for each slice of agar (thickness 1 mm) from the working electrode to the counter electrode. However, here we only show the concentrations of AQDS and AH_2QDS in the first 3 cm of the reacting cell, because no further change of AQDS and AH_2QDS concentration was observed in the last 2 cm.

https://dx.doi.org/10.1021/acs.est.0c02521
Environ. Sci. Technol. 2020, 54, 10646−10653

with the published diffusion-electron hopping model.[46] This estimated electron hopping constant k_{hp} ($\sim 10^8$ L mol^{-1} s^{-1}) was in good agreement with the two-electron self-exchange reaction (i.e., $AQDS^{2-} + 2e^- + 2H^+ \rightarrow AH_2QDS^{2-}$) rate that was calculated by Rosso et al. In their study, the reaction rate for the first (i.e., $AQDS^{2-} + e^- + H^+ \rightarrow AHQDS^{2-\bullet}$) and second (i.e., $AHQDS^{2-\bullet} + e^- + H^+ \rightarrow AH_2QDS^{2-}$) steps of the two-electron self-exchange reaction was determined at $10^{8.19}$ L mol^{-1} s^{-1} and $10^{7.82}$ L mol^{-1} s^{-1}, respectively, which yielded a geometric mean of $10^{8.005}$ L mol^{-1} s^{-1}. Since k_{diff} is smaller than k_{hp}, $k_{overall}$ was rate controlled by the diffusion process. This estimation is consistent with the observed linear dependence of the peak current on the square root of the applied potential scan rate (Figure 3a) and AQDS concentration (SI Figure S5), which supported the diffusion-limited electron-transfer kinetics and verified the application of the diffusion-electron hopping model in our system.

We further performed electrochemical experiments that were combined with spectrophotometric analysis of thin agar slices (1 mm for each slice, Figure 1d) to investigate how electron hopping enhanced diffusion, and thus the overall electron-transfer rate of the diffusion-electron hopping process, in comparison to the case without electron hopping. For an initial AQDS concentration of 25 mmol L^{-1}, a total of 3×10^{-2} mmol AH_2QDS was produced from electrode reduction of AQDS, which reached a maximum transfer distance of 1.6 cm (Figure 4a). Dividing the amount of produced AH_2QDS by the surface area of the electrode (6 cm^2) and the reaction time (3 min to reach the maximum transfer distance), we determined the average AH_2QDS production fluxes ($J_{production}$) to be 3.1×10^{-5} mmol cm^{-2} s^{-1}. For the condition without electron hopping, the concentration gradient for AH_2QDS diffusion was 4.3×10^{-3} mmol cm^{-4} by taking the concentration drop of AH_2QDS into account of the entire transfer distance (SI Figure S9). Such a concentration gradient, however, would only generate a stationary diffusion flux ($J_{diffusion}$) of 2.2×10^{-9} mmol cm^{-2} s^{-1} (estimated based on Fick's first law $J_{diffusion} = -D_0\frac{C}{L}$, $D_0 = 5.5 \times 10^{-7}$ cm^2 s^{-1}, as presented in the last section, $-\frac{C}{L} = 4.3 \times 10^{-3}$ mmol cm^{-4}, represents the concentration gradient). This was much smaller than $J_{production}$ (3.1×10^{-5} mmol cm^{-2} s^{-1}) and therefore not sufficient to sustain the AH_2QDS transfer to the maximum distance at the given reaction time.

The occurrence of electron hopping, on the other hand, divided the diffusion into several short-distance diffusion segments (i.e., eq 4). In each segment, the diffused AH_2QDS was immediately consumed by electron hopping at the encountered surface of the AQDS layer due to the fact that electron hopping is faster than diffusion. Assuming the diffusion flux in each segment ($J_{diffusion,\ seg}$) was the same and equated to the production flux (i.e., $J_{production} = J_{diffusion,seg} = -D_0\frac{C_{seg}}{L_{seg}}$) for a stationary AH_2QDS transfer until the maximum distance, one could obtain a concentration gradient in each segment ($-\frac{C_{seg}}{L_{seg}}$) of 5.0×10^2 mmol cm^{-4} ($-\frac{C_{seg}}{L_{seg}} = \frac{J_{production}}{D_0}$, $J_{production} = 3.1 \times 10^{-5}$ mmol cm^{-2} s^{-1}, $D_0 = 5.5 \times 10^{-7}$ cm^2 s^{-1}). This calculated concentration gradient was 10^5 times higher than that without electron hopping (SI Figure S9a, 4.3×10^{-3} mmol cm^{-4}). As shown above, the estimated electron hopping rate (k_{hp}, $\sim 10^8$ L mol^{-1} s^{-1}) was only 100 times larger than the diffusion rate (k_{diff}, $\sim 10^6$ L mol^{-1} s^{-1}), and the diffusion flux we observed in our experiment ($J_{production}$, 3.1×10^{-5} mmol cm^{-2} s^{-1}) was 10^4 times higher than the diffusion flux ($J_{diffusion}$, 2.2×10^{-9} mmol cm^{-2} s^{-1}). We attributed this nonlinear acceleration of diffusion by electron hopping to the fact that electron hopping accelerates the overall electron-transfer rate by both shortening the diffusion distance and increasing the concentration gradient therefore the diffusion rate in the diffusion segment. Although the increase of the concentration gradient therefore the diffusion rate in the diffusion segment should be linear to the electron hopping rate, the effect of the shortened distance on acceleration is not linearly dependent on the rate of electron hopping.

A similar observation was made in the experiment with an initial AQDS concentration of 50 mmol L^{-1} (Figure 4b) for which the concentration gradient in each segment ($-\frac{C_{seg}}{L_{seg}} = \frac{J_{production}}{D_0} = 1.0 \times 10^4$ mmol cm^{-4}, $J_{production} = 4.6 \times 10^{-3}$ mmol cm^{-2} s^{-1}) was increased 10^6-fold by electron hopping in comparison to the concentration gradient ($-\frac{C}{L} = 1.2 \times 10^{-2}$ mmol cm^{-4}, SI Figure S9b) for the diffusion without electron hopping. This increasing extent of concentration gradient was 10-fold higher than that in the experiment with the initial AQDS concentration of 25 mmol L^{-1}, which was probably due to the shorter diffusion distance in each diffusion segment as a result of the closer contact of AQDS redox centers and thus higher electron hopping frequency at higher concentrations. The redox-center separation decreased from 1.29 to 0.49 nm as the AQDS concentration increased from 25 mmol L^{-1} to 50 mmol L^{-1} (SI Figure S8). Although simplistic, this calculation highlighted the substantial impact of electron hopping on accelerating diffusion fluxes and enhancing the overall electron-transfer kinetics via the AQDS/AH_2QDS couple.

Implications for Particulate NOM Electron Transfer. Here we fit our data to a diffusion-electron hopping model to interpret the electron transfer between immobilized AQDS molecules in agar under diffusion-limited conditions. Such conditions highly resemble the electron-transfer process of particulate NOM for which solid-phase quinone and hydroquinone groups are present. However, a certain number of dissolved NOM molecules with redox-active functional groups are also expected to coexist with the particulate NOM matrix, for example, due to the continuous degradation of particulate natural organic matter.[2,47] After accepting electrons generated from microbial respiration, dissolved quinone groups are transformed to hydroquinone groups, which subsequently diffuse to the particulate NOM due to their high diffusive mobility. Electron hopping between the dissolved hydroquinone and solid-phase quinone groups can largely increase the diffusion concentration gradient and promote the electron transfer of particulate NOM to a rapid and long-distance level. Electron transfer of particulate NOM plays a critical role in element cycling,[12] contaminant transformation,[48] and greenhouse gas emissions.[14] It is thermodynamically favorable to transfer electrons to different terminal electron acceptors including oxygen, iron(III), and manganese(IV) minerals, as well as to nitrate and oxidized S-compounds from high to low reduction potential.[5,49] The diffusion-electron hopping model proposed in this study will be relevant for other studies that address the particulate NOM enhanced electron-transfer

https://dx.doi.org/10.1021/acs.est.0c02521
Environ. Sci. Technol. 2020, 54, 10646−10653

kinetics as well as its impact on environmental electron-transfer networks.

■ ASSOCIATED CONTENT

Supporting Information

The Supporting Information is available free of charge at https://pubs.acs.org/doi/10.1021/acs.est.0c02521.

Fe(II) concentration at sampling location of agar rim and ferrihydrite-mineral core in microbial ferrihydrite reduction experiment with AQDS immobilized in agar as electron shuttle (Figure S1), Fe(III) concentration at agar rim, agar-ferrihydrite interface, and ferrihydrite-mineral core of microbial ferrihydrite reduction experiment with AQDS immobilized in agar as electron shuttle (Figure S2), average microbial ferrihydrite reduction rate with different concentrations of AQDS immobilized in agar as electron shuttles (Figure S3), cyclic voltammogram of AQDS in agar (Figure S4), linear relationship of peak current and AQDS concentration at different potential scan rates (Figure S5), formal potential of different concentrations of AQDS (Figure S6), peak current and overpotential as functional of potential scan rate at different concentrations of AQDS (Figure S7), estimated distance between two AQDS molecules with different amounts of AQDS immobilized in agar (Figure S8), and concentration gradient of AH_2QDS in the electrochemical experiment combined with spectrophotometric analysis of thin agar slices (Figure S9) (PDF)

■ AUTHOR INFORMATION

Corresponding Author

Andreas Kappler − *Geomicrobiology, Center for Applied Geosciences, University of Tübingen, D-72074 Tübingen, Germany;* orcid.org/0000-0002-3558-9500; Phone: +49-7071-2974992; Email: andreas.kappler@uni-tuebingen.de

Authors

Yuge Bai − *Geomicrobiology, Center for Applied Geosciences, University of Tübingen, D-72074 Tübingen, Germany*

Tianran Sun − *Environmental Biotechnology, Center for Applied Geosciences, University of Tübingen, D-72074 Tübingen, Germany*

Largus T. Angenent − *Environmental Biotechnology, Center for Applied Geosciences, University of Tübingen, D-72074 Tübingen, Germany;* orcid.org/0000-0003-0180-1865

Stefan B. Haderlein − *Environmental Mineralogy and Chemistry, Center for Applied Geosciences, University of Tübingen, D-72074 Tübingen, Germany*

Complete contact information is available at: https://pubs.acs.org/10.1021/acs.est.0c02521

Author Contributions

‖Y.B. and T.S. contributed equally to this work.

Notes

The authors declare no competing financial interest.

■ ACKNOWLEDGMENTS

This study was supported by a grant from the German Research Foundation (KA1736/37-1). T.S. and L.A. acknowledge support from the Alexander von Humboldt Foundation in the framework of the Alexander von Humboldt Professorship endowed by the Federal Ministry of Education and Research in Germany. We would like to thank Ellen Roehm for the development of the agar-solidified experimental setup and the preliminary tests. We thank Paula Eisnecker, Ellen Roehm, and Manuel Schad for their help to set up the experiments. Many thanks to Lars Grimm and Franziska Schaedler for their technical support in the lab.

■ REFERENCES

(1) Stevenson, F. J. *Humus chemistry: genesis, composition, reaction*; Wiley: New York, U.S.A., 1994.

(2) Sparks, D. L. *Environmental soil chemistry*; Academic Press: Boston, U.S.A., 2003; DOI: 10.1016/B978-0-12-656446-4.X5000-2.

(3) Lan, S.; Wang, X. M.; Yang, P.; Qin, Z. J.; Zhu, M. Q.; Zhang, J.; Liu, F.; Tan, W. F.; Huang, Q. Y.; Feng, X. H. The catalytic effect of AQDS as an electron shuttle on Mn(II) oxidation to birnessite on ferrihydrite at circumneutral pH. *Geochim. Cosmochim. Acta* **2019**, *247*, 175−190.

(4) Lovley, D. R.; Coates, J. D.; BluntHarris, E. L.; Phillips, E. J. P.; Woodward, J. C. Humic substances as electron acceptors for microbial respiration. *Nature* **1996**, *382* (6590), 445−448.

(5) Roden, E. E.; Kappler, A.; Bauer, I.; Jiang, J.; Paul, A.; Stoesser, R.; Konishi, H.; Xu, H. F. Extracellular electron transfer through microbial reduction of solid-phase humic substances. *Nat. Geosci.* **2010**, *3* (6), 417−421.

(6) Sposito, G. Electron Shuttling by Natural Organic Matter: Twenty Years After. *ACS Symp. Ser.* **2011**, *1071*, 113−127.

(7) Balch, J.; Guéguen, C. Determination of diffusion coefficients of dissolved organic matter in the Churchill River estuary system, Hudson Bay (Canada). *Environ. Chem.* **2015**, *12* (2), 253−260.

(8) Orita, A.; Verde, M. G.; Sakai, M.; Meng, Y. S. A biomimetic redox flow battery based on flavin mononucleotide. *Nat. Commun.* **2016**, *7* (1), 13230.

(9) Phalak, P.; Chen, J.; Carlson, R. P.; Henson, M. A. Metabolic modeling of a chronic wound biofilm consortium predicts spatial partitioning of bacterial species. *BMC Syst. Biol.* **2016**, *10* (1), 90.

(10) Glasser, N. R.; Saunders, S. H.; Newman, D. K. The colorful world of extracellular electron shuttles. *Annu. Rev. Microbiol.* **2017**, *71*, 731−751.

(11) Six, J.; Paustian, K.; Elliott, E. T.; Combrink, C. Soil structure and organic matter: I. Distribution of aggregate-size classes and aggregate-associated carbon. *Soil Sci. Soc. Am. J.* **2000**, *64* (2), 681−689.

(12) Lau, M. P.; Sander, M.; Gelbrecht, J.; Hupfer, M. Solid phases as important electron acceptors in freshwater organic sediments. *Biogeochemistry* **2015**, *123* (1−2), 49−61.

(13) Tan, W. B.; Yuan, Y.; Zhao, X. Y.; Dang, Q. L.; Yuan, Y.; Li, R. F.; Cui, D. Y.; Xi, B. D. Soil solid-phase organic matter-mediated microbial reduction of iron minerals increases with land use change sequence from fallow to paddy fields. *Sci. Total Environ.* **2019**, *676*, 378−386.

(14) Gao, C.; Sander, M.; Agethen, S.; Knorr, K. H. Electron accepting capacity of dissolved and particulate organic matter control CO_2 and CH_4 formation in peat soils. *Geochim. Cosmochim. Acta* **2019**, *245*, 266−277.

(15) Nielsen, L. P.; Risgaard-Petersen, N.; Fossing, H.; Christensen, P. B.; Sayama, M. Electric currents couple spatially separated biogeochemical processes in marine sediment. *Nature* **2010**, *463* (7284), 1071−1074.

(16) Piepenbrock, A.; Kappler, A. Humic Substances and Extracellular Electron Transfer. In *Microbial Metal Respiration*; Gescher, J., Kappler, A., Eds.; Springer: Berlin, Heidelberg, Germany, 2013; pp 107−128, DOI: 10.1007/978-3-642-32867-1_5.

(17) Rosso, K. M.; Smith, D. M. A.; Wang, Z. M.; Ainsworth, C. C.; Fredrickson, J. K. Self-exchange electron transfer kinetics and reduction potentials for anthraquinone disulfonate. *J. Phys. Chem. A* **2004**, *108* (16), 3292−3303.

(18) Narayanan, J.; Xiong, J. Y.; Liu, X. Y. Determination of agarose gel pore size: Absorbance measurements vis other techniques. *J. Phys.: Conf. Ser.* **2006**, *28*, 83−86.
(19) Bai, Y.; Mellage, A.; Cirpka, O. A.; Sun, T.; Angenent, L. T.; Haderlein, S. B.; Kappler, A. AQDS and redox-active NOM enables microbial Fe(III)-mineral reduction at cm-scales. *Environ. Sci. Technol.* **2020**, *54*, 4131−4139.
(20) Jiang, J.; Kappler, A. Kinetics of microbial and chemical reduction of humic substances: Implications for electron shuttling. *Environ. Sci. Technol.* **2008**, *42* (10), 3563−3569.
(21) Klupfel, L.; Piepenbrock, A.; Kappler, A.; Sander, M. Humic substances as fully regenerable electron acceptors in recurrently anoxic environments. *Nat. Geosci.* **2014**, *7* (3), 195−200.
(22) Piepenbrock, A.; Schroder, C.; Kappler, A. Electron transfer from humic substances to biogenic and abiogenic Fe(III) oxy-hydroxide minerals. *Environ. Sci. Technol.* **2014**, *48* (3), 1656−1664.
(23) Hegler, F.; Posth, N. R.; Jiang, J.; Kappler, A. Physiology of phototrophic iron(II)-oxidizing bacteria: implications for modern and ancient environments. *FEMS Microbiol. Ecol.* **2008**, *66* (2), 250−60.
(24) Viollier, E.; Inglett, P. W.; Hunter, K.; Roychoudhury, A. N.; Van Cappellen, P. The ferrozine method revisited: Fe(II)/Fe(III) determination in natural waters. *Appl. Geochem.* **2000**, *15* (6), 785−790.
(25) Orsetti, S.; Laskov, C.; Haderlein, S. B. Electron transfer between iron minerals and quinones: Estimating the reduction potential of the Fe(II)-goethite surface from AQDS speciation. *Environ. Sci. Technol.* **2013**, *47* (24), 14161−14168.
(26) Chen, J.; Gu, B. H.; Royer, R. A.; Burgos, W. D. The roles of natural organic matter in chemical and microbial reduction of ferric iron. *Sci. Total Environ.* **2003**, *307* (1−3), 167−178.
(27) Piepenbrock, A.; Dippon, U.; Porsch, K.; Appel, E.; Kappler, A. Dependence of microbial magnetite formation on humic substance and ferrihydrite concentrations. *Geochim. Cosmochim. Acta* **2011**, *75* (22), 6844−6858.
(28) Shimizu, M.; Zhou, J.; Schröder, C.; Obst, M.; Kappler, A.; Borch, T. Dissimilatory reduction and transformation of ferrihydrite-humic acid coprecipitates. *Environ. Sci. Technol.* **2013**, *47* (23), 13375−13384.
(29) Roden, E. E.; Urrutia, M. M. Influence of biogenic Fe(II) on bacterial crystalline Fe(III) oxide reduction. *Geomicrobiol. J.* **2002**, *19* (2), 209−251.
(30) Roden, E. E.; Wetzel, R. G. Kinetics of microbial Fe(III) oxide reduction in freshwater wetland sediments. *Limnol. Oceanogr.* **2002**, *47* (1), 198−211.
(31) Urrutia, M. M.; Roden, E. E.; Fredrickson, J. K.; Zachara, J. M. Microbial and surface chemistry controls on reduction of synthetic Fe(III) oxide minerals by the dissimilatory iron-reducing bacterium *Shewanella alga*. *Geomicrobiol. J.* **1998**, *15* (4), 269−291.
(32) Huskinson, B.; Marshak, M. P.; Suh, C.; Er, S.; Gerhardt, M. R.; Galvin, C. J.; Chen, X. D.; Aspuru-Guzik, A.; Gordon, R. G.; Aziz, M. J. A metal-free organic-inorganic aqueous flow battery. *Nature* **2014**, *505* (7482), 195−198.
(33) Liao, S. C.; Zong, X.; Seger, B.; Pedersen, T.; Yao, T. T.; Ding, C. M.; Shi, J. Y.; Chen, J.; Li, C. Integrating a dual-silicon photoelectrochemical cell into a redox flow battery for unassisted photocharging. *Nat. Commun.* **2016**, *7*, 11474.
(34) Bai, Y.; Subdiaga, E.; Haderlein, S. B.; Knicker, H.; Kappler, A. High-pH and anoxic conditions during soil organic matter extraction increases its electron-exchange capacity and ability to stimulate microbial Fe(III) reduction by electron shuttling. *Biogeosciences* **2020**, *17* (3), 683−698.
(35) Dahms, H. Electronic conduction in aqueous solution. *J. Phys. Chem.* **1968**, *72* (1), 362−364.
(36) Ruff, I.; Friedrich, V. J. Transfer diffusion. I. Theoretical. *J. Phys. Chem.* **1971**, *75* (21), 3297−3302.
(37) Ruff, I.; Friedrich, V. J.; Demeter, K.; Csillag, K. Transfer diffusion. II. Kinetics of electron exchange reaction between ferrocene and ferricinium ion in alcohols. *J. Phys. Chem.* **1971**, *75* (21), 3303−3309.
(38) Blauch, D. N.; Saveant, J. M. Dynamics of electron hopping in assemblies of redox centers. Percolation and diffusion. *J. Am. Chem. Soc.* **1992**, *114* (9), 3323−3332.
(39) Marcus, R. A. On the theory of oxidation-Reduction reactions involving electron transfer. *J. Chem. Phys.* **1956**, *24* (5), 966−978.
(40) Bard, A. J.; Faulkner, L. R. *Electrochemical Methods: Fundamentals and Applications*; Wiley: India, 2001.
(41) Akhoury, A.; Bromberg, L.; Hatton, T. A. Interplay of electron hopping and bounded diffusion during charge transport in redox polymer electrodes. *J. Phys. Chem. B* **2013**, *117* (1), 333−342.
(42) Pirbadian, S.; El-Naggar, M. Y. Multistep hopping and extracellular charge transfer in microbial redox chains. *Phys. Chem. Chem. Phys.* **2012**, *14* (40), 13802−13808.
(43) Subramanian, P.; Pirbadian, S.; El-Naggar, M. Y.; Jensen, G. J. Ultrastructure of *Shewanella oneidensis* MR-1 nanowires revealed by electron cryotomography. *Proc. Natl. Acad. Sci. U. S. A.* **2018**, *115* (14), E3246−E3255.
(44) Batchelor-McAuley, C.; Li, Q.; Dapin, S. M.; Compton, R. G. Voltammetric characterization of DNA intercalators across the full pH range: Anthraquinone-2,6-disulfonate and anthraquinone-2-sulfonate. *J. Phys. Chem. B* **2010**, *114* (11), 4094−4100.
(45) Ji, X.; Banks, C. E.; Silvester, D. S.; Wain, A. J.; Compton, R. G. Electrode kinetic studies of the hydroquinone-benzoquinone system and the reaction between hydroquinone and ammonia in propylene carbonate: Application to the indirect electroanalytical sensing of ammonia. *J. Phys. Chem. C* **2007**, *111* (3), 1496−1504.
(46) Sato, K.; Ichinoi, R.; Mizukami, R.; Serikawa, T.; Sasaki, Y.; Lutkenhaus, J.; Nishide, H.; Oyaizu, K. Diffusion-cooperative model for charge transport by redox-active nonconjugated polymers. *J. Am. Chem. Soc.* **2018**, *140* (3), 1049−1056.
(47) Lehmann, J.; Kleber, M. The contentious nature of soil organic matter. *Nature* **2015**, *528*, 60.
(48) Zheng, W.; Liang, L. Y.; Gu, B. H. Mercury reduction and oxidation by reduced natural organic matter in anoxic environments. *Environ. Sci. Technol.* **2012**, *46* (1), 292−299.
(49) Aeschbacher, M.; Graf, C.; Schwarzenbach, R. P.; Sander, M. Antioxidant properties of humic substances. *Environ. Sci. Technol.* **2012**, *46* (9), 4916−4925.

https://dx.doi.org/10.1021/acs.est.0c02521
Environ. Sci. Technol. 2020, 54, 10646−10653